

Structure-dependent mobility of a dry aqueous foam flowing along two parallel channels

S. A. Jones,¹ B. Dollet,¹ Y. Méheust,² S. J. Cox,³ and I. Cantat¹

¹*Institut de Physique de Rennes (UMR CNRS 6251), Université de Rennes 1, 35042 Rennes, France*

²*Géosciences (UMR CNRS 6118), Université de Rennes 1, 35042 Rennes, France*

³*Institute of Mathematics and Physics, Aberystwyth University, Aberystwyth SY23 1BN, UK*

(Dated: Version 5)

The velocity of a two-dimensional aqueous foam has been measured as it flows through two parallel channels, at a constant overall volumetric flow rate. The flux distribution between the two channels is studied as a function of the ratio of their widths. A peculiar dependence of the velocity ratio on the width ratio is observed when the foam structure in the narrower channel is either single staircase or bamboo. In particular, discontinuities in the velocity ratios are observed at the transitions between double and single staircase and between single staircase and bamboo. A theoretical model accounting for the viscous dissipation at the solid wall and the capillary pressure across a film pinned at the channel outlet predicts the observed non-monotonic evolution of the velocity ratio as a function of the width ratio. It also predicts quantitatively the intermittent temporal evolution of the velocity in the narrower channel when it is so narrow that film pinning at its outlet repeatedly brings the flow to a near stop.

I. INTRODUCTION

Aqueous foams are present in many manufactured goods, from personal hygiene products to processed foods, but also play an important role in many industrial processes^{1,2}. Some of these processes involve the injection of a foam into the Earth's surface or subsurface, in particular to enhance oil recovery³ or as a carrier fluid for soil remediation processes⁴. This latter application is recent and particularly promising as there are many expected advantages of injecting a foam rather than a single phase fluid in the polluted soil. It allows a large reduction of the needed volume of liquid for a given injection volume, while maintaining a very good compatibility with the surfactants already used for soil remediation^{5,6}. There is also the potential capacity for the selective transport of material by the foam, in the form of particles of polluted soil or colloidal pollutant, in the same manner as in ore separation by froth flotation. In addition, if bioremediation of a soil is required, the transport of air along with the liquid in a foam may enhance the efficiency of any biological activity⁷.

In both enhanced oil recovery and soil remediation a foam flows through a porous material with a complex geometry. Being able to predict how a foam flows in a confined, tortuous, geometry is therefore of great importance, and has been studied for many years⁸⁻¹¹. Laboratory-scale experiments most commonly study the flow through a cylindrical column of a porous material, consisting of either a model system, such as packed glass beads, or a sample of soil, sand or rock from the field.

Bertin *et al.*¹² obtained a puzzling experimental result during testing of a heterogeneous porous medium: the (interstitial) velocity of the foam front invading a saturated porous medium was larger in the low permeability region than in the high permeability region. The mobility of the foam is classically quantified through an *effective viscosity*, defined as the viscosity of the Newtonian fluid that would flow at the same velocity in the same geometry under an identical pressure head⁸. For a bubble size larger than the characteristic pore size, even in heterogeneous porous media, the foam is organized in trains of lamellae^{8,9}. In this case, Kovscek and Bertin¹³ have shown theoretically that the specific dissipation associated with this structure leads to an effective viscosity of the foam that scales with the permeability K of the porous medium as a power law with an exponent $3/2$. This key ingredient, also observed in¹⁴, is at the origin of the faster invasion of the low permeability regions of heterogeneous porous media when foam is used instead of a Newtonian fluid. However, the complex models developed to address this type of behaviour^{13,15} involve many

different assumptions about local processes (local dissipation laws, local foam structure, bubble production and coalescence rate). Full visualisations of foam flows in model porous media are therefore urgently needed to validate and improve these theoretical approaches.

Two-dimensional diphasic flows in porous media have been investigated extensively in the last 25 years, allowing researchers to map out the rich phenomenology of flow regimes^{16–19}, to finely characterize their dynamics^{20,21}, and gain partial understanding of how the pore scale dynamics results in macroscopic transport properties²². These experimental studies have relied on disordered porous media consisting of networks of linear channels, monolayers of glass beads, or, more recently, microfluidic devices²³. However, the limit in which the liquid fraction of the foam is very low has seen little investigation, although bubble formation in this limit has been investigated in²⁴, for air in pure water or in a solution of surfactants. This dry foam limit involves specific foam stability issues, making the problem more complicated.

Here we investigate the basic flow behaviour of a dry two-dimensional foam as it moves through two parallel linear channels enclosed in a larger cell (see Fig. 1). This simple system mimics the bifurcation of a large pore into two smaller ones (at the entrance to the two channels), and the reconnection of two small pores into a larger one (at the exit). The width of each channel is uniform along its length, and the two widths can be varied systematically for given bubble size and combined channel width. With this very simple geometry we can investigate how the total foam flux, which is imposed upstream, is distributed into the two channels. We believe this represents an important local step toward the understanding of the flux distributions in heterogeneous porous media.

The pressure drop along such a channel has been measured for a single channel in a similar geometry²⁵ and explored theoretically with the viscous froth model^{26–29}. In this study we use these established results to determine the pressure drop from the velocity and structure of the foam, and show that the dissipation law used in¹³ is valid for simple trains of lamellae. However, when the foam structure is more complex, with several bubbles across the channel section, we show how to modify the model to correctly reproduce our experimental results. This correction comes from the dependence of the friction force on the film orientation²⁵. We also show that, even for channels much longer than the bubble size, end effects are important, and they are much greater for channels venting to open air. We rationalise these end effects by taking into account the competition between viscous and capillary forces.

The plan of the paper is as follows. Our methods are given in §II and the experimental results

for enclosed and open-ended channels are described in §III. In §IV we discuss the theoretical model that we compare to experiments in §V. Finally, we draw conclusions in §VI.

II. METHODOLOGY

A. Experimental Set-Up

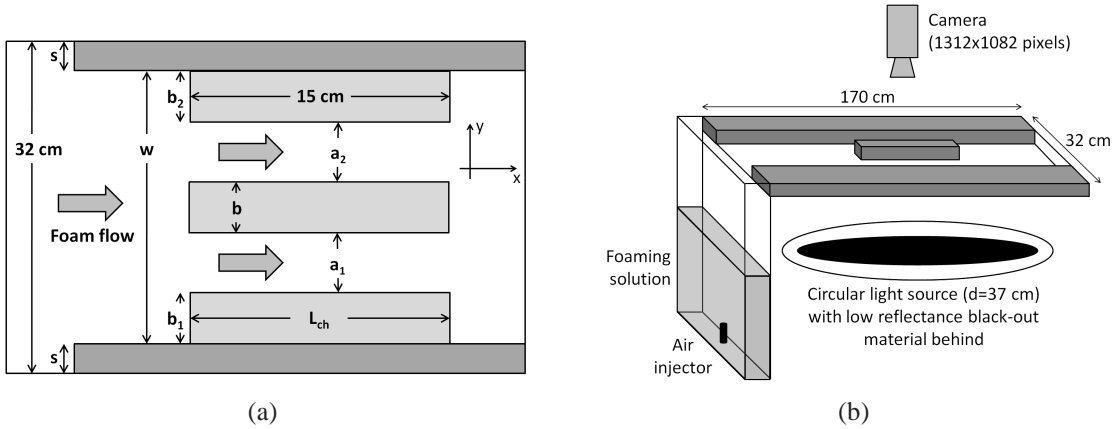


FIG. 1. Schematic representations of (a) the experimental channels, with a_1 and a_2 the channel widths and b the separation distance between channels, and (b) the complete experimental setup.

The double-channel flow experiments were carried out in a Hele-Shaw cell with a plate separation of either $h = 0.1$ cm or $h = 0.2$ cm. Rectangular obstacles cut from polycarbonate sheet were placed within the Hele-Shaw cell to form two parallel channels. The channel length L_{ch} is 15 cm for all experiments, and the values of a_1 , a_2 , b , b_1 , b_2 and s , defined on Fig. 1(a), could be changed to meet individual test requirements. The central obstacle could be moved sideways to study asymmetric channel configurations. For the experiment shown in this paper, we chose $b_1 = b_2 = b$ and $(a_1 + a_2)/w = 2/5$, unless different values are specified. The obstacles were positioned either half-way along the channel, as shown in Fig. 1(b), so that they were completely surrounded by the flowing foam (‘enclosed channel’ configuration) or they could be positioned at the end of the channel with the foam venting to the atmosphere (‘open-ended channel’ configuration).

The foaming solution used in all tests was 10 g/l sodium dodecyl sulfate (SDS) in ultra-pure water, with surface tension $\gamma = 36.8 \pm 0.3$ mN/m, as measured in³⁰, and viscosity $\mu = 1 \times 10^{-3}$ Pa·s. Foam was created by blowing nitrogen, at a rate of $Q = 100$ cm³/min, through a single nozzle in the base of the vertical foam production cell (Fig. 1(b)). This produced a monodisperse foam

with a typical bubble volume Ω deduced from the contact area A between the bubble and the top glass plate, through the relation $\Omega = hA$. We define the *equivalent bubble radius* as $R = \sqrt{A/\pi}$.

The liquid fraction was estimated from the rate of decrease of the level of the foaming solution³⁰, since the gas flow rate is known. Values in the range 0.01 to 0.02 were obtained for all the tests presented here.

The Hele-Shaw cell was backlit by a circular (diameter = 37 cm) fluorescent tube with a central dark background so that soap films appear white with good contrast. The motion of the foam was recorded using a 1312×1082 pixel digital video camera running at 25 fps. A typical image of the foam in the enclosed channel configuration is given in Fig. 2.

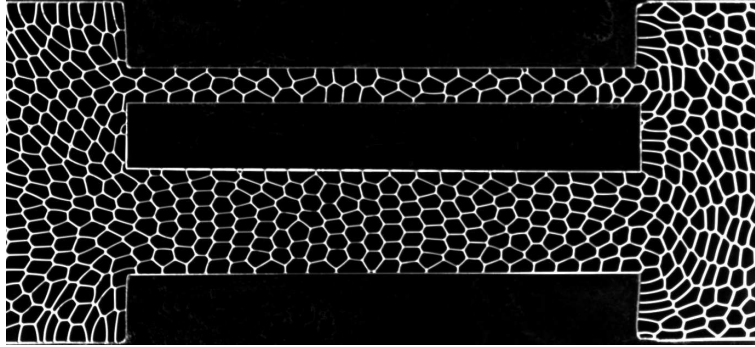


FIG. 2. Image of the foam flow from left to right through two enclosed channels of length 15 cm in a test section of length 22 cm.

B. Image processing

Basic image processing, thresholding and skeletonisation of the foam images was carried out using the ImageJ software package. The resultant images were then analysed using an in-house analysis program, described fully in³¹. The image treatment procedure tracks individual bubbles to compute the velocity distribution within the test section over a rectangular mesh of 40×50 boxes. The foam flow in the channels is a plug flow, with a uniform velocity, except in a small domain at the entrance and at the exit. We define the velocities V_1 and V_2 as the velocities in the central part of the channels 1 and 2 (outside the entrance and exit domains), averaged over time. The time and space average velocity in the channel of width w , before the separation into two channels, is called V_0 .

III. EXPERIMENTAL RESULTS

Two asymmetric channel configurations were investigated: the ‘enclosed channel’ and the ‘open-ended channel’. The former is relevant to the continuous flow of a foam through a channel within a porous medium, while the latter is appropriate when considering the penetration of a foam into an air-filled porous medium, as well as to the flow of a foam along a channel that emerges into a larger void within a porous medium.

A. Enclosed Channel

The enclosed channel tests were carried out with a Hele-Shaw plate separation of $h = 0.1$ cm. The average bubble area, A , was in the range 0.19 to 0.20 cm², with an equivalent diameter of $2R \approx 0.5$ cm and a maximum polydispersity index of 25%.

The first set of tests were performed with channel dimensions of $b = b_1 = b_2 = 2$ cm and $a_1 + a_2 = 4$ cm, resulting in $w = 10$ cm. The central obstacle was moved from a central position $a_1 = a_2 = 2$ cm to one side in increments of 0.1 or 0.2 cm, to give a range of different a_1 and a_2 , with a_2 denoting the width of the narrow channel.

Examples of the foam structures observed, with the names that we use for them, are shown in Fig. 3. For channel widths much larger than the bubble radius R , a random foam is observed. For a channel just slightly wider than $2R$, the foam adopts a crystalline structure with only a few columns of bubbles (double staircase and staircase structure). Below a certain channel width the staircase structure becomes unstable and a transition towards a bamboo structure is observed³². These structures are sensitive to both the average bubble size and the polydispersity of the foam, especially in the transition region between staircase and bamboo, where small increases or decreases in the bubble size can push the structure either way. In general, a bamboo foam is obtained when the channel width is such that $a_2 \leq 2R$.

Tests were also carried out with $b = 2$ cm and $b_1 = b_2 = 0$ cm (see Fig. 1), giving a channel width of $w = 6$ cm. These ‘straight-walled’ tests were carried out to determine whether the up-stream corners introduced by the inclusion of the two side obstacles had any effect on the flow behaviour within the channels. No difference in the flow behaviour was found between the ‘stepped’ and the straight-walled tests, and the two sets of results are presented together in the following.

In Fig. 4(a) we plot the ratio of the average bubble velocities in each of the two channels as

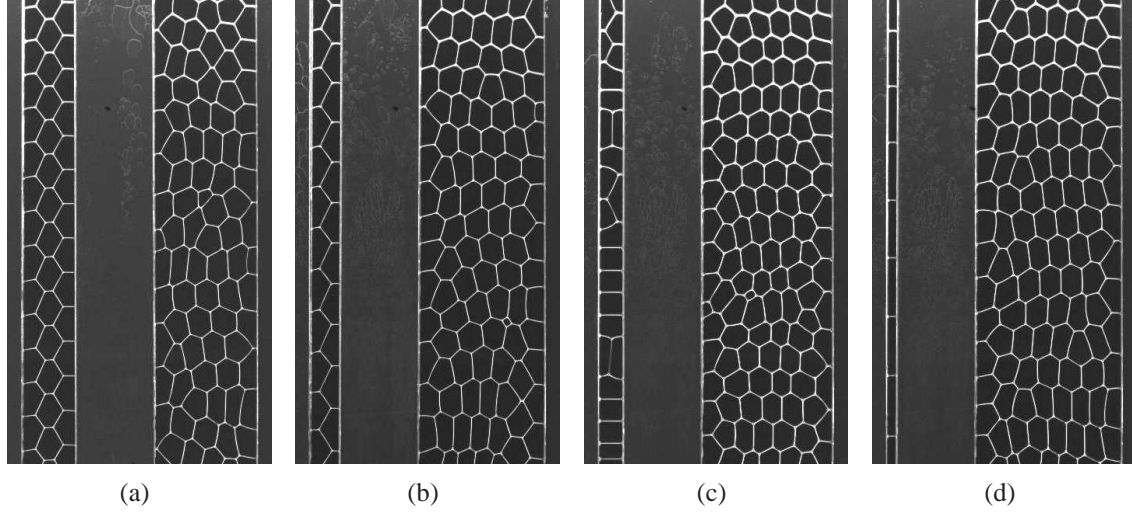
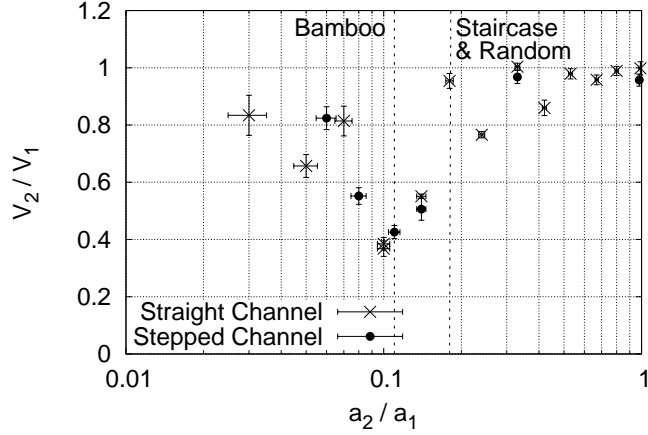


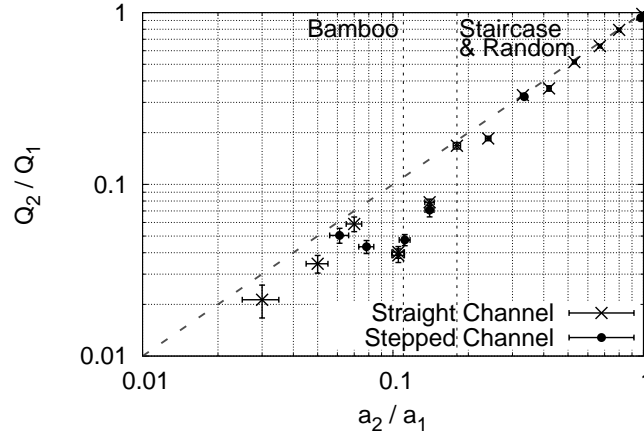
FIG. 3. Images of foam flow through asymmetric enclosed channels (flow from bottom to top), with widths satisfying $a_1 + a_2 = 4$ cm. As the smaller channel becomes narrower, the foam structure explores a range of ordered and disordered arrangements. Ordered arrangements are shown for narrow channel widths of (a) $a_2 = 1.33$ cm, (b) $a_2 = 0.72$ cm, (c) $a_2 = 0.59$ cm and (d) $a_2 = 0.22$ cm, resulting in double staircase, single staircase, mixed staircase/wide bamboo, and narrow bamboo structures, respectively. The wider channel contains a random two-dimensional foam in each case.

a function of the ratio of channel widths a_2/a_1 . If two or more bubbles span the narrow channel there is little difference between the velocities in both channels ($V_2/V_1 \approx 1$). However, once the transition to a bamboo foam occurs, the flow in the narrow channel becomes much slower than in the larger one. The velocity ratio reaches a minimum for a narrow channel width of the order of $a_{\min} = 1.5R$. For very small channel widths, the velocity in the narrow channel increases again (analogously to the findings of Bertin *et al.*¹²), recovering to within 20% of the velocity in the wide channel.

The corresponding ratio of the fluxes in the two channels is shown as a function of the channel width ratio in Fig. 4(b). This plot is obtained by simply multiplying the velocity ratios of Fig. 4(a) by the factor a_2/a_1 . Consequently, in the staircase/random regime the flux ratio is equal to the channel width ratio, but once the transition to bamboo structure occurs there is a significant drop in the flux in the narrow channel. As the channel width ratio is reduced from 0.1 to 0.07 the flux ratio then increases again. It is significant that when the foam has a bamboo structure there is an interval in which reducing the size of the narrow channel causes an *increase* in the flux through the narrow channel.



(a)



(b)

FIG. 4. Dependence of (a) the velocity ratio, V_2/V_1 , and (b) the flux ratio, Q_2/Q_1 , on the channel width ratio, a_2/a_1 , for the enclosed channels. The bubble size is $R = 0.25$ cm and $a_1 + a_2 = 4$ cm. The dotted vertical lines indicate the limits of the transition zone in which a mixture of single staircase and bamboo foam was observed in the narrow channel. The regions of the graph in which only bamboo or where only staircase or random foams were observed are labeled.

B. Open-Ended Channels

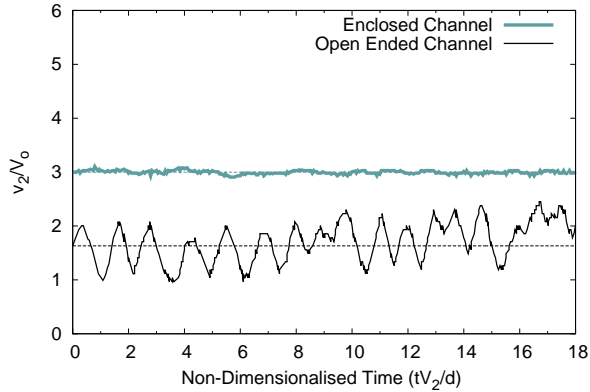
In an open-ended channel test, the obstacles were positioned at the end of the Hele-Shaw cell (with plate separation, $h = 0.2$ cm) so that the foam passing through the two channels vented to the open air. Tests were carried out for a_2 ranging from 2 cm down to 0.1 cm, and for three different total fluxes in the system, 100, 50 or 25 cm^3/min . In these experiments A was in the range 0.25 to 0.29 cm^2 , with an equivalent diameter of $2R \approx 0.6$ cm, and with a maximum polydispersity index of 25%.

Similar results to those for the enclosed channels were obtained when staircase or random foam structures were observed in both channels. However, once the transition to bamboo foam had occurred in the narrow channel an important end effect was observed, with the introduction of significant velocity oscillations in the narrow channel at lower values of a_2 . In this case, all the films of the bamboo structure move at the same velocity $v_2(t)$, that varies with time around its average value V_2 . Fig. 5 shows $v_2(t)$, divided by the reference velocity V_0 (upstream of the channels), as a function of time, for two different bamboo structures. For the enclosed tests there is very little, if any, variation of the velocity with time. For the open ended tests however, there are significant variations in the velocity with time, with the amplitude of these oscillations increasing as the channel width decreases. In Fig. 5, the time is rescaled by d/V_2 , with d the average distance between two lamellae in the bamboo structure. A lamella reaches the end of channel 2 every $t = d/V_2$. This period coincides with the period of velocity oscillations, which are due to film pinning at the exit.

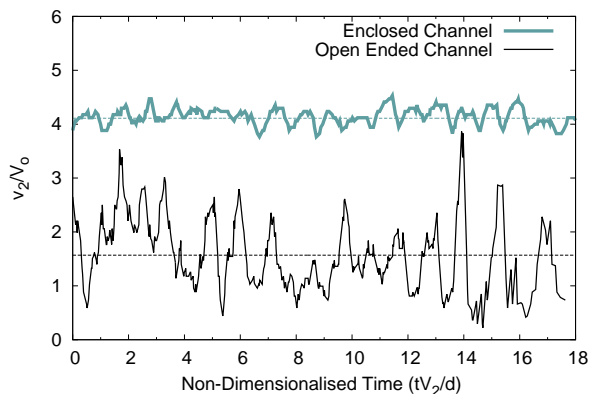
The ratio of the time-averaged velocities in the two channels is plotted as a function of the ratio of the channel widths in Fig. 6, which should be compared to Fig. 4(a). The large oscillations in the velocity of a bamboo foam in the narrow channel lead to large error bars in this region. There is a wide scatter in the data obtained at different fluxes when the foam has a bamboo structure, but no clear dependency has been evidenced.

IV. MODEL

The pressure distribution in the experiment is shown schematically in Fig. 7. We define two reference pressures: P_{up} , the pressure upstream of the channels, where the pressure distribution perpendicular to the direction of flow is still homogeneous; and P_{down} , which for the open-ended channels is atmospheric pressure, and for the enclosed channels is the pressure downstream of the channels where the flow becomes uniform again. The pressure drop $P_{\text{up}} - P_{\text{down}}$ can be decomposed into five contributions: (i) $P_{\text{up}} - P_{\text{in}^-}$, due to both the viscous friction on the plates before entering the channel, and to the elasto-plastic stress in the foam, arising from the strong deformations that occur in the foam in this region; (ii) $P_{\text{in}^-} - P_{\text{in}^+}$ due to a possible high film curvature at the channel entrance, inducing a Laplace pressure drop (as the bubble size may be of the order of the channel size this contribution can not be described in the frame of a continuum model and requires separate treatment); (iii) $P_{\text{in}^+} - P_{\text{out}^-}$ due only to the viscous force exerted by the channel



(a)



(b)

FIG. 5. Velocity, non-dimensionalised by the reference velocity V_0 , versus dimensionless time for both the enclosed and open-ended channels. (a) For a channel of width 0.38 cm and (b) for a channel of width 0.12 cm. Large fluctuations are observed for open-ended channels. The mean value V_2 for each case is indicated with a dashed line. The velocity in the enclosed-channel data is offset by +2 to improve clarity.

walls, since we have confirmed that the flow is plug-like in the two channels; (iv) $P_{\text{out}^-} - P_{\text{out}^+}$, the equivalent of (ii) for the exit; and finally, (v) $P_{\text{out}^+} - P_{\text{down}}$, the equivalent of (i) for the exit.

The aim of this section is to explain these different contributions, allowing us to interpret the experimental velocity measurements in §V.

A. Viscous forces

The pressure drop associated with the flow of a bamboo foam moving at velocity $\mathbf{v} = V\mathbf{e}_x$ in a channel oriented in the direction \mathbf{e}_x is directly related to the total length of meniscus in contact with the wall. In this geometry, the viscous force exerted by the wall is indeed localised along the

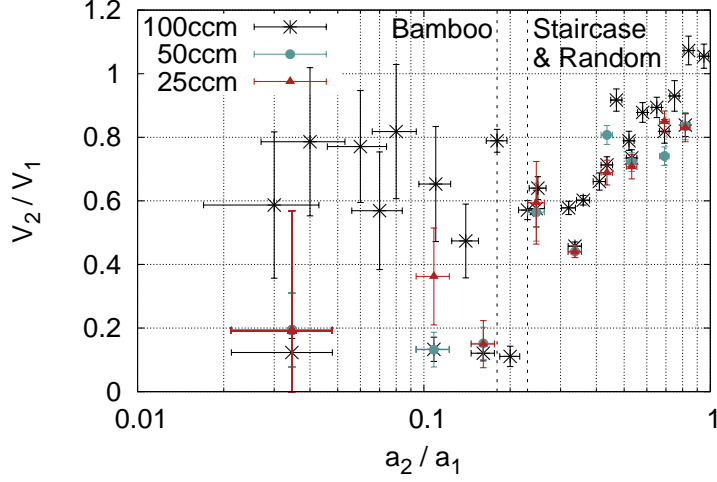


FIG. 6. Velocity ratio, V_2/V_1 , plotted as a function of the channel width ratio, for open-ended channels.

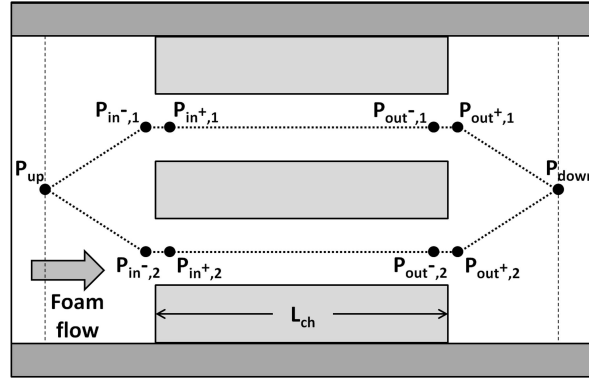


FIG. 7. Schematic diagram of the experiment showing the points at which the pressures P_{up} , P_{in^-} , P_{in^+} , P_{out^+} , P_{out^-} and P_{down} are defined.

meniscus and it can be expressed, per unit length of meniscus, as

$$\mathbf{f}_{\text{film}} = -\lambda\gamma Ca^{2/3} \mathbf{e}_x, \quad (1)$$

where λ is a dimensionless prefactor, γ is the surface tension and Ca the capillary number, defined as $Ca = \eta V/\gamma$, η being the dynamic viscosity of the foaming solution.

However, for a more general 2D foam structure, the menisci can have an arbitrary orientation θ with respect to the channel orientation (see Fig. 8). The viscous force per unit length of meniscus decreases as θ increases. Rather than the total length L of meniscus, it was shown by Cantat et al.²⁵ that the projected length perpendicular to the flow determines the total viscous force exerted on a moving film, in agreement with their experimental observations. Similarly, a general vectorial

relation for the viscous force was proposed in²⁶:

$$\mathbf{f} = f(\mathbf{v} \cdot \mathbf{n})\mathbf{n}, \quad (2)$$

where \mathbf{n} is the normal to the film. f is the scalar viscous force, obtained from eq. (1), and is defined by:

$$f(\mathbf{v} \cdot \mathbf{n}) = -\lambda\gamma(\eta\mathbf{v} \cdot \mathbf{n}/\gamma)^{2/3}. \quad (3)$$

For a 2D foam moving without deformation at a uniform velocity $\mathbf{v} = V\mathbf{e}_x$ in a channel of cross-sectional area $S = ah$, the viscous pressure drop ΔP_{visc} can be calculated from the force balance on the foam, with inertia negligible in our parameter range. Using eq. (2) projected along the \mathbf{e}_x direction and summing the contributions from all the menisci in contact with the bounding plates, we obtain

$$\Delta P_{\text{visc}} = \frac{\gamma\lambda}{S} \left(\frac{\eta V}{\gamma} \right)^{2/3} \sum_i \left(L^{(i)} \cos^{5/3} \theta^{(i)} \right) = \frac{\gamma\lambda}{S} Ca^{2/3} \sum_i \left(L^{(i)} \cos^{5/3} \theta^{(i)} \right), \quad (4)$$

where $L^{(i)}$ and $\theta^{(i)}$ are the length of the meniscus denoted by index i , and its orientation with respect to the channel axis respectively.

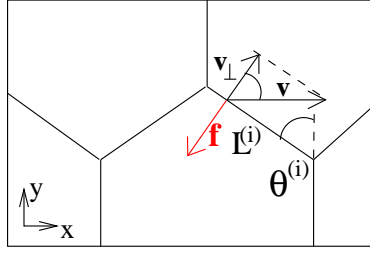


FIG. 8. A meniscus of length $L^{(i)}$ and orientation $\theta^{(i)}$, travelling at velocity \mathbf{v} . The normal velocity, $\mathbf{v}_\perp = (\mathbf{v} \cdot \mathbf{n})\mathbf{n}$, and the viscous force acting on the film, \mathbf{f} , are indicated.

The experiments in²⁵ gave a value of $\lambda \approx 38 \pm 10\%$ for both bamboo and single staircase structures in a similar geometry. Raufaste *et al.*²⁹ extended this work to a more extensive 2D random foam, and also considered the effect of liquid fraction. Their measurements yielded the empirical relation:

$$\lambda = (10.27 \pm 0.52) \left(\frac{R_p}{\sqrt{A}} \right)^{-0.48 \pm 0.02}, \quad (5)$$

where R_p is the radius of curvature of the meniscus at the wall, and A is the bubble area as seen from

above. This relation holds for R_p/\sqrt{A} between 0.01 and 0.35, corresponding to liquid fractions between 0.01% to 30%. The ratio R_p^2/A can be calculated from the liquid fraction ϕ of the foam using²⁹

$$\frac{R_p^2}{A} = \frac{\phi}{2C_v + C_{hw}\frac{\mathcal{P}}{h}},$$

where h is the plate separation in the Hele-Shaw cell and \mathcal{P} is the bubble perimeter. C_v and C_{hw} are constants associated with the shapes of the vertical and horizontal Plateau borders respectively; for a purely hexagonal foam they are²⁹ $C_v = \sqrt{3} - \pi/2$ and $C_{hw} = 2 - \pi/2$.

However, for a foam in a narrow channel the structure is generally not hexagonal: there are pentagonal bubbles at the walls, and in a very narrow channel the bubbles are rectangular (bamboo). C_{hw} is independent of the individual bubble shape, but C_v varies with changes to the bubble geometry. Following²⁹, it has been derived by us to be $1 + \sqrt{3}/2 - \pi/2$ for regular pentagonal bubbles touching the cell side and $2 - \pi/2$ for bamboo bubbles (touching both cell sides).

Using the relevant parameters for each foam structure, depending on the liquid fraction and the bubble shape, we obtain values of λ for our experiments in the range 34 to 58.

B. Pressure drop for the bamboo structure

For the bamboo structure, eq. (4) can be rewritten explicitly as a function of the bubble volume Ω . The length of meniscus touching the wall is, per bubble, $L = 2(a + h)$, with an angle $\theta = 0$; a and h are the width and height of the channel respectively. The distance between two films is $d = \Omega/(ah)$ and so the number of films in a channel of length L_{ch} is L_{ch}/d . We therefore predict the pressure gradient along a channel to be

$$\frac{\Delta P_{\text{visc,bam}}}{L_{\text{ch}}} = \frac{\eta V \lambda}{Ca^{1/3}} \frac{2(a+h)}{\Omega}. \quad (6)$$

Kovscek et al¹³ consider the case $a = h$ and the apparent viscosity of the foam η_f is determined as defined by the relation

$$\frac{\Delta P_{\text{visc}}}{L_{\text{ch}}} = \frac{\eta_f}{K} V_d, \quad (7)$$

where K is the absolute permeability of the medium (as defined for a Newtonian fluid), and V_d is the Darcy (or filtration, or superficial) velocity, which in our case is the mean cross-sectional velocity: $V_d = \psi V$, $\psi = (a_1 + a_2)/w$ being the porosity. The permeability K scales as a^2 , i.e.

$K = \beta a^2$, with β a constant depending on the geometry. Note that β could differ considerably from unity if the aspect ratio of the pore cross section itself is very different from unity. Using these notations, relation (6) can thus be transformed into

$$\frac{\Delta P_{\text{visc,bam}}}{L_{\text{ch}}} = \frac{\eta V_d}{\psi K} \frac{\lambda}{Ca^{1/3}} \frac{4K^{3/2}}{\Omega \beta^{1/2}}, \quad (8)$$

which by comparison with eq. (7) shows that the effective viscosity of the foam scales with $K^{3/2}$:

$$\eta_f = \eta \frac{\lambda}{Ca^{1/3}} \frac{4K^{3/2}}{\Omega \psi \beta^{1/2}}. \quad (9)$$

Hence the improved foam penetration observed in the low permeability domains in the experiments of Bertin et al.¹² results from this $K^{3/2}$ dependence. We also note that increasing the overall flow rate (i.e. increasing Ca) improves the efficiency of the displacement, as measured in³³.

C. Pressure drop for a staircase structure and a randomly-oriented hexagonal 2D foam

Eq. (6), however, does not predict the significant velocity decrease at the staircase to bamboo transition, when the amount of meniscus in contact with the wall suddenly increases, making the sum in eq. (4) much larger at given bubble volume and channel width^{25,34}.

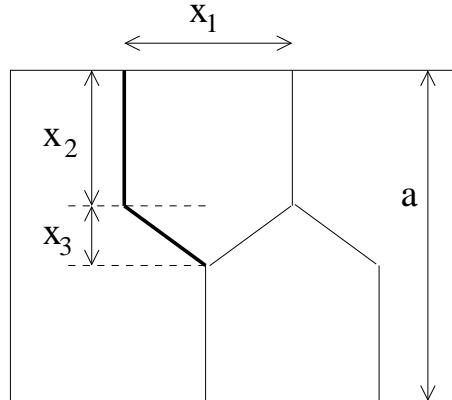


FIG. 9. Sketch of a staircase structure.

The different edge lengths and orientation of the staircase can be determined from the bubble volume Ω and the channel width a and thickness h . Three characteristic lengths are depicted in Fig. 9: x_1 , x_2 and x_3 ; they are related to each other through the relations $2x_2 + x_3 = a$ and $x_1(x_2 + x_3/2) = \Omega/h$, whence $x_1 = (2\Omega)/(ah)$. Neglecting the deformation of the bubble induced

by viscous forces³⁵, we assume that the angles between the edges are $2\pi/3$. We can then deduce $x_1 = 2\sqrt{3}x_3$, which immediately leads to $x_3 = \Omega/(\sqrt{3}ah)$.

A length L_{ch} of foam consists of $N = hL_{\text{ch}}a/\Omega$ bubbles. The meniscus network in contact with the plates has N vertical segments of length h , $2N$ segments of length x_2 and $2N$ segments of length x_3 , at an angle $\theta = \pi/3$ (see Fig. 9). Finally, eq. (4) leads to:

$$\frac{\Delta P_{\text{visc, stair}}}{L_{\text{ch}}} = \frac{\eta V \lambda}{Ca^{1/3}} \left(\frac{a+h}{\Omega} + \frac{2^{1/3}-1}{3^{1/2}S} \right). \quad (10)$$

The pressure drop induced by the motion of a randomly-oriented hexagonal 2D foam is obtained by averaging the contribution of regular hexagons over all possible orientations. We assumed $a \gg h$ and $a \gg \sqrt{(\Omega/h)}$ so that the correction arising from the lateral boundaries become negligible.

$$\frac{\Delta P_{\text{visc, rand}}}{L_{\text{ch}}} = 1.99 \frac{\eta V \lambda}{Ca^{1/3}} (\Omega h)^{-1/2}. \quad (11)$$

D. Capillary pressure

We next determine the additional pressure drop induced by a bubble exiting the channel. When a film emerges from a channel, we have observed that it remains pinned to the exit corners, and is progressively deformed by the constant gas flux, until it eventually breaks or depins. We consider the capillary pressure across the film, ΔP_{cap} , to be given by the Young-Laplace equation:

$$\Delta P_{\text{cap}} = 2\gamma \left(\frac{1}{r_1} + \frac{1}{r_2} \right), \quad (12)$$

where r_1 and r_2 are the two radii of curvature of this bubble shape. As an illustrative example, we computed the film shape with Surface Evolver³⁶ for the case of a bamboo film exiting a rectangular channel, with an arbitrary value of $h = 0.8a$, pinned on the channel boundary (Fig. 10). The pressure reaches its maximal value $\Delta P_{\text{cap}}^M \sim 2\gamma(1/a + 1/h)$ for an external volume $V \sim a^3$ before decreasing slowly as the external volume increases. This maximal pressure has to be overcome before the flow in the channel can proceed. After rupture or depinning this film is replaced by another film and, after a short transient, the pressure reaches a value close to its maximal value again.

In general, the capillary pressure at the exit from the channel is

$$\Delta P_{\text{cap}} = P_{\text{out}^-} - P_{\text{out}^+} = 2\gamma \left(\left\langle \frac{1}{r_1} \right\rangle + \left\langle \frac{1}{r_2} \right\rangle \right), \quad (13)$$

where $\langle 1/r_1 \rangle$ is a film's time-averaged curvature in the horizontal plane and $\langle 1/r_2 \rangle$ its time-averaged curvature in the vertical plane parallel to the channel's side walls.

Instead of doing extensive numerical simulations, and in order to obtain analytical predictions, we choose to use an approximated but simple value for this capillary pressure drop. For the enclosed channel experiments, the top and bottom plates are smooth and the film is free to slide on them. We thus use $\langle 1/r_2 \rangle = 1/h$ for the open-ended channel and $\langle 1/r_2 \rangle = 0$ for the enclosed structure. For the bamboo structure $\langle 1/r_1 \rangle \approx 1/a$ for both open-ended and enclosed cases. For the other structures, it is more difficult to give a precise analysis of the bubble shape at the exit. A good order of magnitude is obtained with $\langle 1/r_1 \rangle \approx 1/R$ for the staircase structure (R being the typical bubble radius, see §II A) and $\langle 1/r_1 \rangle \approx 0$ for a random foam, as in this situation $a \gg h$ and pinning on the side walls is expected to have a negligible influence.

The capillary pressure at the entrance $P_{in,+} - P_{in,-}$ is more difficult to predict and is discussed in section V A.

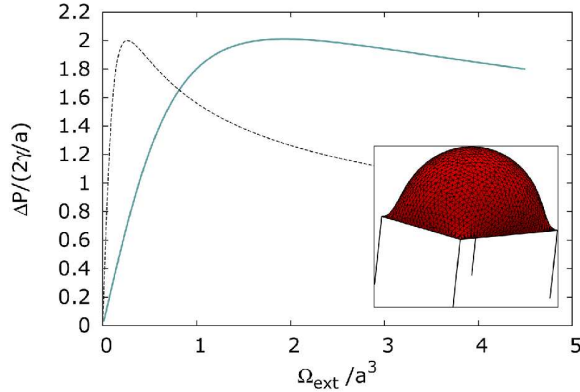


FIG. 10. Surface Evolver³⁶ simulation of a bamboo film emerging from a channel with a rectangular cross-section $a \times h$ with $h = 0.8a$. Main graph: Ratio of the capillary pressure across the film to $2\gamma/a$, as a function of the bubble volume external to the channel Ω_{ext} divided by a^3 . For comparison, we show the result obtained for a cylindrical tube of radius $a/2$ (dashed line). Inset: Image of the emergent film. The film is pinned all around the exit from the channel.

E. Pressure drop upstream of the entrance

The foam velocity is very inhomogeneous close to the channel entrance, with both stagnation points and high-velocity domains. The foam is thus strongly sheared and internal elastic and viscous stresses govern the pressure fields in addition to the friction on the plates discussed in §IV A. As the velocity field in front of each channel is different, $P_{\text{up}} - P_{\text{in}^-,1}$ could *a priori* significantly differ from $P_{\text{up}} - P_{\text{in}^-,2}$. To test this assumption, we carried out experiments with two channels of equal width in an off-centre position in the Hele-Shaw cell ($a_1 = a_2$, $b_1 = 0$ cm, $b_2 = 4$ cm), in a open-ended geometry. We obtained the same velocity in both channels within 10%. This implies that $P_{\text{in}^-,1} - P_{\text{down}}$ and $P_{\text{in}^-,2} - P_{\text{down}}$ are close, *i.e.* $(P_{\text{in}^-,1} - P_{\text{in}^-,2}) / (P_{\text{in}^-,1} - P_{\text{down}}) \ll 1$. This indicates that even a very asymmetrical entrance leads to a negligible difference between $P_{\text{in}^-,1}$ and $P_{\text{in}^-,2}$, and we will consider both values as equal in the following.

V. COMPARISON OF THE MODEL WITH THE EXPERIMENTAL MEASUREMENTS

A. Enclosed channel

In order to predict the velocity ratio between the two channels, we take into account both the viscous and the capillary pressure at the exit, discussed in §IV A and IV D, with the assumption that $\Delta P_{\text{visc},1} + \Delta P_{\text{cap},1} = \Delta P_{\text{visc},2} + \Delta P_{\text{cap},2}$. Using eqs. (4) and (13), we deduce the velocity ratio as a function of the physico-chemical parameters, the experimental foam structure and the velocity in the wide channel:

$$\frac{V_2}{V_1} = \frac{1}{S_2^{3/2}} \left[S_1 - \frac{2}{Ca_1^{2/3} r_2} \right]^{3/2}, \quad (14)$$

with

$$S_j = \frac{\lambda}{a_j h} \sum_i \left(L_j^{(i)} \cos^{5/3} \theta_j^{(i)} \right), \quad j \in \{1, 2\}. \quad (15)$$

To derive this expression, we have used two facts: that the terms containing r_1 cancel out since the two channels have the same height, and that $\langle 1/r_2 \rangle \approx 0$ in the largest channel since the foam is always random there. The relative importance of the viscous and capillary terms depends on the velocity, or equivalently on the capillary number in the wide channel Ca_1 , and hence depends on

the total flux. It also depends on the channel length, through the summation over all menisci in contact with the walls.

This prediction is plotted in Fig. 11 (dots, red online) and shows a reasonable agreement with most experimental values. However, for the smallest channels, the prediction overestimates the velocity in the narrow channel. One reason for this may be an overestimation of λ , as the value given in eq. (5) was measured with a different foaming solution²⁹.

Additionally, as noted above, the behaviour of the foam at the entrance to the narrower channel can be quite complex, as shown in Fig. 12, with transient staircase structures being formed that then undergo a transition to bamboo (Figs. 12(a)-(c)). These transition occur through topological rearrangements, called T1s, during which the bubble contact network is modified. We also observed that films attached to bubbles outside the narrow channel could become greatly extended along the centre of the channel (Fig. 12 (d)). This stretch persists until a T1 occurs, and can result in a bubble being split into two parts if the corner of the obstacle pierces the film prior to the T1. It is very difficult to quantify these effects, but there is potentially an induced correction factor for $P_{in,+} - P_{in,-}$ in the pressure balance equation for the narrowest channels.

Most notably the velocity ratio varies non-monotonically with the width ratio, with sudden jumps at the structure transitions, an important feature that can be explained by considering the viscous pressure drop only. Eqs. (6), (10) and (11) allow us to derive the following analytical predictions for the velocity ratio as a function of the channel width ratio for every possible structure in the narrow channel of width a and thickness h (a random foam is always assumed in the wider channel):

$$\frac{V_{\text{bamb}}}{V_{\text{rand}}} = \left(\frac{0.99\sqrt{A}}{a_2 + h} \right)^{3/2}, \quad (16)$$

$$\frac{V_{\text{stair}}}{V_{\text{rand}}} = \left(\frac{1.99}{\sqrt{A}} \right)^{3/2} \left(\frac{a_2 + h}{A} + \frac{2^{1/3} - 1}{\sqrt{3}a_2} \right)^{-3/2}. \quad (17)$$

These predictions are plotted in Fig. 11 together with the experimental data. The model captures the non-monotonous behavior, in particular the velocity jump at each structure transition; this is strikingly different from the behavior of a Newtonian fluid, which shows a smooth decrease in velocity ratio with decreasing channel width ratio. We overestimate the velocity in the narrowest channels due to the neglect of the capillary pressure, however this purely viscous model is expected

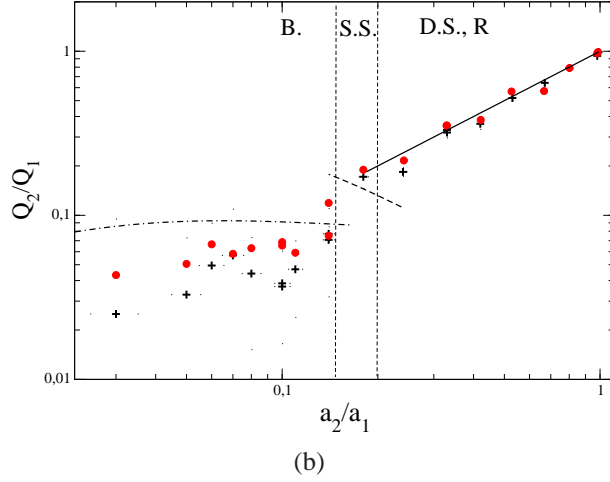
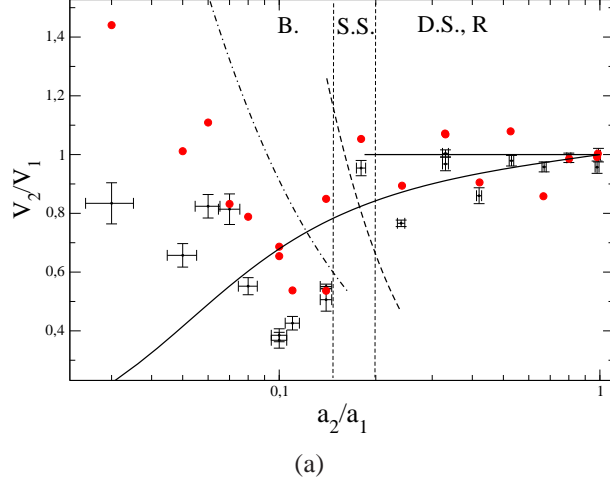


FIG. 11. (a) Comparison of the experimental data of Fig. 4 with theoretical predictions. Analytical prediction: horizontal solid line - random foam structure (R) in the narrow channel; dashed line - staircase structure (S.S.), eq. (17); dotted-dashed line - bamboo structure (B. S.), eq. (16) ($A = 0.19 \text{ cm}^2$, $h = 0.1 \text{ cm}$ and $a_2 = 4x/(1+x)$ in cm, with $x = a_2/a_1$). The functions are plotted in the domains of existence of the corresponding structure, as observed experimentally. The vertical dashed lines that separate these domains are not strict frontiers, and some fluctuations are observed. In the “random domain”, adjacent to the staircase domain, one data point corresponds to a double staircase structure (D.S.), for which a special treatment would lead to a better theoretical prediction. The prediction of eq. (14), determined from the experimental values of the foam structure and the velocity in the wide channel, is given as \bullet . The curved solid line is the velocity ratio expected for a Newtonian fluid³⁷. The analytical expression is given in Annex. (b) Same data for the fluxes (without the result for a Newtonian fluid).

to be valid for very long channels, for which the viscous pressure drop becomes much higher than the capillary pressure at the channel ends. The model predicts a large increase of V_2 as a_2/a_1 becomes small, but above a certain velocity the films break³⁸, which limits the accessible velocity range. It should also be noted that the plateau at larger a_2/a_1 ratios (i. e., when the foam structure

is double staircase or random in both channels) is expected from relation (11) to be independent of the channels' widths.

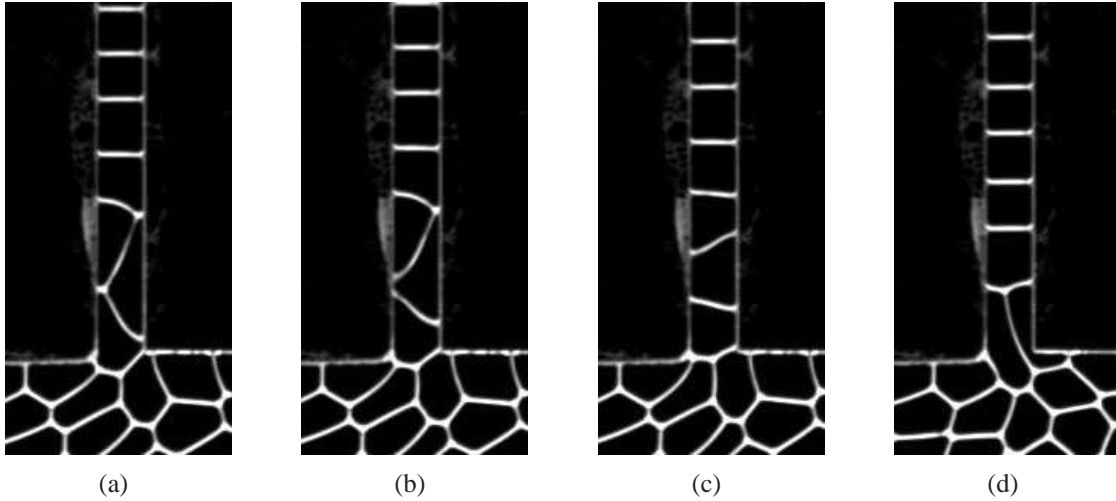


FIG. 12. Images of the foam entering a narrow channel ($a_2 = 0.49$ cm) to form a wide bamboo structure. The average bubble area is 0.25 ± 0.05 cm², with an equivalent diameter of 0.51 ± 0.06 cm. Images (a)-(c) show three consecutive frames ($\Delta t = 0.05$ s) of an experiment in which a transient staircase structure is formed at the entrance to the channel before making the transition to a wide bamboo structure. Image (d) shows a single film being stretched down the centre of the channel – this phenomena only occurs when the foam forms a wide bamboo structure.

B. Intermittency of the flow triggered by the capillary pressure drop

For an open-ended channel, the shape of any film external to the Hele-Shaw cell evolves with time. As discussed in §IV D, the Surface Evolver was used to calculate this changing pressure drop as a film emerges from the channel, and a graph of the dimensionless pressure drop against the dimensionless external volume is given in Fig. 10. This curve has a maximum, and if an experiment is carried out with a low total flux in the system, a situation can be reached where the driving pressure in the system is not enough to get past this maximum, and the flow in the narrow channel is therefore halted.

This phenomena was observed for $a_2 = 0.13$ cm with a total flux in the system of 25 cm³/min. The foam remained stationary within the narrow channel until the external bubble burst due to film drainage, resulting in a rapid spike in velocity before decay back down to zero. The resulting velocity trace for this low flux case is given in Fig. 13.

The velocity suddenly increases when the bubble bursts (at time 0 in Fig. 13) and reaches a

steady value v_0 imposed by the pressure drop ΔP_0 , according to

$$\Delta P_0 = N f(v_0) \frac{2(a+h)}{ah}, \quad (18)$$

where N is the number of bamboo films present in the tube and $f(v_0)$ is the scalar viscous force previously defined in eq. (3). It should be noted that, as the flux in the wide channel is much larger than the one in the narrow channel, it can be considered equal to the imposed total flux, and therefore ΔP_0 can be considered constant. This means that v_0 is governed by the imposed total flux. Eventually, at a time t_1 , another film reaches the end of the tube and becomes pinned. The film velocity $v(t)$ begins to decrease, as the capillary pressure increases and a new blocked situation is reached.

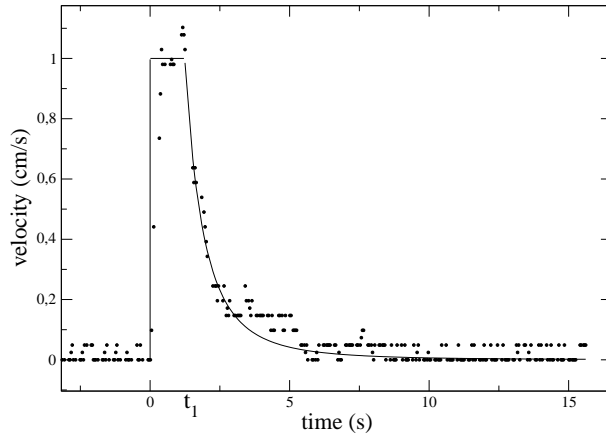


FIG. 13. Velocity of a bamboo film in a narrow channel as a function of time. • Experimental data. Solid line, for $t > t_1$: prediction of eq. (25) $v(t) = v_0 [1 + (t - t_1)/\tau]^{-3}$, with the adjustable parameter $\tau = 2s$. v_0 is the maximal velocity, reached by the lamella between $t = 0$, the time at which a pinned bubble burst, and $t_1 = 1.24s$, the time at which a new film was pinned at the channel outlet.

The exact shape of the bubble when the meniscus is pinned at the exit of the channel is not well-controlled and, in order to get a simple analytical prediction for the intermittent velocity, we assume the simplest possible shape for the pinned contour: a circle of radius α . We checked that the analogous 2-D calculation for a rectangle of size $h \times 2\alpha$, with $h \gg \alpha$ leads to a very similar prediction, up to a prefactor close to 1. The prediction is also very close to the full numerical calculation for $\Omega_{\text{ext}}/a^3 \lesssim 1$ (Fig.10).

As the bubble reaches the exit and remains pinned on the circle of radius α , its shape is a

spherical cap with radius of curvature R . The external volume is given by

$$\Omega_{\text{ext}} = \frac{\pi}{2} R (1 - \cos \theta_{pin}) \left[\frac{R^2}{3} (1 - \cos \theta_{pin})^2 + \alpha^2 \right] \quad (19)$$

with $\sin \theta_{pin} = \alpha/R$. In the limit $R \gg \alpha$ we get

$$\frac{1}{R} = \frac{4\Omega_{\text{ext}}}{\pi\alpha^4}. \quad (20)$$

Since the overall pressure drop is fixed at ΔP_0 , the viscous pressure drop along the channel is simply ΔP_0 less the capillary pressure across the bubble interface:

$$\Delta P_{\text{visc}}(t) = \Delta P_0 - \frac{4\gamma}{R} = \Delta P_0 - \frac{16\Omega_{\text{ext}}\gamma}{\pi\alpha^4}. \quad (21)$$

The external volume of the bubble is also related to the flux:

$$\Omega_{\text{ext}} = \int_{t_1}^t \pi\alpha^2 v(t) dt, \quad (22)$$

which allows us to deduce the viscous pressure drop as a function of time

$$\Delta P_{\text{visc}}(t) = \Delta P_0 - \frac{16\gamma}{\alpha^2} \int_{t_1}^t v(t) dt. \quad (23)$$

Using eq. (4) and assuming that the number of menisci does not change during the duration of the bubble growth, we have $v_0^{2/3}/\Delta P_0 = v(t)^{2/3}/\Delta P_{\text{visc}}(t)$, which results in

$$\left(\frac{v(t)}{v_0} \right)^{2/3} = 1 - \frac{16\gamma}{\alpha^2 \Delta P_0} \int_{t_1}^t v(t') dt'. \quad (24)$$

After differentiating with respect to time, eq. (24) becomes a simple differential equation that can be solved by separation of variables, leading to:

$$\frac{v(t)}{v_0} = \left[1 + \frac{8\gamma v_0 (t - t_1)}{\alpha^2 \Delta P_0} \right]^{-3} = \left[1 + \frac{t - t_1}{\tau} \right]^{-3}, \quad (25)$$

where the characteristic time for the velocity decay is $\tau = \alpha^2 \Delta P_0 / (8\gamma v_0)$. As shown in Fig. 13, a good agreement is obtained for $\tau = 2$ s. This corresponds to $\alpha = 0.6$ cm. The corresponding disc area is 1.13 cm^2 whereas the actual section of the channel is 0.026 cm^2 . The discrepancy

is larger than expected, for unidentified reasons. The pressure oscillation is thus only understood qualitatively, and would require a specific study, with a shape visualisation at the exit, which is beyond the scope of this paper.

In this situation, the average velocity in the narrow channel strongly depends on the bubble behavior at the exit (pinning, bursting etc.), which was not controlled in the open-ended experiments. This explains the dispersion in the data at low width ratios in Fig. 6, in the regime where flow can, notably, be arrested in the narrow channel.

VI. CONCLUSION

In this paper, we have measured the velocity of a two-dimensional foam as it flows through two parallel channels. We have varied the relative width of the channels at fixed combined width, in order to investigate how changes in the foam structure inside the narrower channel influence the distribution of fluxes between the two channels, for a given imposed total volumetric flow rate. Two geometric configurations were used, one with channels enclosed inside a larger Hele-Shaw cell, and another one in which the two channels vent to the open air. They are respectively relevant to (i) the continuous flow of a foam through a channel within a porous medium, and (ii) to the imbibition of a foam into an air-filled porous medium or to the flow of a foam along a channel that emerges into a void much larger than the typical bubble size.

In the bamboo regime the velocity in the narrow channel decreases as the channel width is increased. This brings a direct experimental evidence of the better foam penetration in the smallest pores that had already been observed in real 3D porous media. However, when the narrow channel becomes larger than the bubble size, the structure goes from a bamboo structure to a staircase structure. This structure transition induces an abrupt increase of the velocity in the narrow channel which dominates over the slow decrease of the velocity with increasing channel width previously discussed. Eventually, when the narrow channel is in the random foam regime (with bubble size much smaller than channel width), the velocity becomes independent of the channel width. A theoretical model accounting only for the viscous dissipation at the contact between the complex menisci network and the bounding plates allows us to qualitatively predict the smooth decrease of the velocity in the narrow channel, and the sudden jumps at the structure transitions observed when the narrow channel width increases. Taking into account corrections induced by the capillary pressure across the films pinned at the channel outlet leads to an almost quantitative velocity

prediction, although the theory overestimates to some extent the velocity in the narrower channel.

This work improves our understanding of the better foam penetration in the smallest pores and underlines the strong influence of the local organisation of the foam. For configurations of open-ended channels with a very narrow channel, the pinning effect at the channel exit is much more important and the flow of the bamboo foam becomes intermittent. The flow is periodically brought close to a halt while the capillary pressure across the bubble pinned at the channel outlet builds up, until that bubble bursts or depins.

Prospects for future work arising from this study include the study of foam dissipation at an intersection of two channels, and, more generally, the study of foam flow in experimental geometries that resemble the geometry of a random porous medium more closely.

APPENDIX

Calculation of ratio of mean velocities in the Newtonian case.

The ratio of the mean velocities for a Newtonian fluid, calculated from a solution of Poiseuille flow³⁷ is

$$\frac{V_2}{V_1} = \frac{\left[1 - \sum_{n,\text{odd}}^{\infty} \frac{1}{n^5} \frac{192}{\pi^5} \frac{h}{a_2} \tanh\left(n\pi\frac{a_2}{2h}\right) \right]}{\left[1 - \sum_{n,\text{odd}}^{\infty} \frac{1}{n^5} \frac{192}{\pi^5} \frac{h}{a_1} \tanh\left(n\pi\frac{a_1}{2h}\right) \right]} .$$

This prediction is plotted with the experimental data in figure 11. The curve shows a smooth drop off in the velocity as the channel width ratio decreases.

ACKNOWLEDGMENTS

We are grateful to Alain Faisant, Jean-Charles Potier and Patrick Chasle for technical support, and to CNRS, the Région Bretagne and the Institut Universitaire de France for financial support. SJC acknowledges financial support from the project PIAP-GA-2009-251475-HYDROFRAC.

REFERENCES

- ¹D. Weaire and S. Hutzler, *The physics of foams*, Oxford Univ. Press, Oxford, 2000.
- ²I. Cantat, S. Cohen-Addad, F. Elias, F. Graner, R. Höhler, O. Pitois, F. Rouyer, and A. Saint-Jalmes, *Les mousses. Structure et dynamique*, Belin, Paris, 2010.

- ³W. R. Rossen, *Foam in enhanced oil recovery*, pages 413–465, Dekker, Cleveland, 1996.
- ⁴S. Wang and C. N. Mulligan, An evaluation of surfactant foam technology in remediation of contaminated soil, *Chemosphere* **57**(9), 1079 – 1089 (2004).
- ⁵C. N. Mulligan, R. N. Yong, and B. F. Gibbs, Surfactant-enhanced remediation of contaminated soil: a review, *Engineering Geology* **60**(1-4), 371 – 380 (2001).
- ⁶C. N. Mulligan and F. Eftekhari, Remediation with surfactant foam of PCP-contaminated soil, *Engineering Geology* **70**(3-4), 269 – 279 (2003), Third British Geotechnical Society Geoenvironmental Engineering Conference.
- ⁷R. Rothmel, R. Peters, E. St. Martin, and M. DeFlaun, Surfactant Foam/Bioaugmentation Technology for In Situ Treatment of TCE-DNAPLs, *Environmental Science and Technology* **32**, 1667–1675 (1998).
- ⁸G. Hirasaki and J. B. Lawson, Mechanisms of foam flow in porous media : apparent viscosity in smooth capillaries, *Soc. Pet. Eng. J.* **25**, 176–188 (1985).
- ⁹W. R. Rossen, Theory of mobilization pressure gradient of flowing foams in porous media: I. Incompressible foam, *J. Colloid Interface Sci.* **136**(1), 1 – 16 (1990).
- ¹⁰A. Kovscek and C. Radke, Fundamentals of foam transport in porous media, Technical Report, univ. California Berkeley (1993).
- ¹¹K. G. Kornev, A. V. Neimark, and A. N. Rozhkov, Foam in porous media: thermodynamic and hydrodynamic peculiarities, *Adv. Colloid Interface Sci.* **82**, 127 – 187 (1999).
- ¹²H. Bertin, O. Apaydin, L. Gastanier, and A. Kovscek, Foam flow in heterogeneous porous media: Effect of Cross Flow, *J. Soc. Petrol. Eng.* **4**, 75– 82 (1999).
- ¹³A. R. Kovscek and H. J. Bertin, Foam Mobility in Heterogeneous Porous Media, *Transp. Porous. Med.* **52**, 17–35 (2003).
- ¹⁴A. H. Falls, G. J. Hirasaki, T. W. Patzek, D. A. Gauglitz, D. D. Miller, and T. Ratulowski, Development of a mechanistic foam simulator: the population balance and generation by snap-off, *SPE reservoir engineering* **3**, 884–892 (1988).
- ¹⁵D. Du, P. Zitha, and F. Vermolen, Numerical Analysis of Foam Motion in Porous Media Using a New Stochastic Bubble Population Model, *Transp. Porous. Med.* **86**, 461–474 (2011).
- ¹⁶R. Lenormand and C. Zarcone, Invasion Percolation in an Etched Network: measurement of a Fractal Dimension, *Phys. Rev. Lett.* **54**(20), 2226–2229 (1985).
- ¹⁷R. Lenormand, E. Touboul, and C. Zarcone, Numerical models and experiments on immiscible displacements in porous media, *J. Fluid Mech.* **189**, 165–187 (1988).

- ¹⁸K. J. Måløy, J. Feder, and T. Jøssang, Viscous fingering fractals in porous media, *Phys. Rev. Lett.* **55**(24), 2688–2691 (1985).
- ¹⁹Y. Méheust, G. Løvoll, K. J. Måløy, and J. Schmittbuhl, Interface scaling in a two-dimensional porous medium under combined viscous, gravity, and capillary effects, *Phys. Rev. E* **66**(5), 051603 (2002).
- ²⁰K. J. Måløy, L. Furuberg, J. Feder, and T. Jøssang, Dynamics of slow drainage in porous-media, *Phys. Rev. Lett.* **68**(14), 2161–2164 (1992).
- ²¹R. Toussaint, G. Løvoll, Y. Méheust, J. Schmittbuhl, and K. J. Måløy, Influence of pore-scale disorder on viscous fingering during drainage, *EPL* **71**(4), 583–589 (2005).
- ²²R. Toussaint, K. J. Måløy, Y. Méheust, G. Løvoll, M. Jankov, G. Schäfer, and J. Schmittbuhl, Two-Phase Flow: Structure, Upscaling, and Consequences for Macroscopic Transport Properties, *Vadose Zone J.* **11** (2012).
- ²³C. Cottin, H. Bodiguel, and A. Colin, Drainage in two-dimensional porous media: From capillary fingering to viscous flow, *Phys. Rev. E* **82**, 046315 (2010).
- ²⁴A. Kavscek, G.-Q. Tang, and C. Radke, Verification of Roof snap-off as a foam-generation mechanism in porous media at steady state, *Colloids Surf. A* **302**(1-3), 251 – 260 (2007).
- ²⁵I. Cantat, N. Kern, and R. Delannay, Dissipation in foam flowing through narrow channels, *EPL* **65**, 726–732 (2004).
- ²⁶N. Kern, D. Weaire, A. Martin, S. Hutzler, and S. J. Cox, The two dimensionnal viscous froth model for foam dynamics, *Phys. Rev. E* **70**, 041411 (2004).
- ²⁷T. E. Green, A. Bramley, L. Lue, and P. Grassia, Viscous froth lens, *Phys. Rev. E* **74**(5), 051403 (2006).
- ²⁸P. Grassia, G. Montes-Atenas, L. Lue, and T. E. Green, A foam film propagating in a confined geometry: Analysis via the viscous froth model, *Eur. Phys. J. E* **25**, 39–49 (2008).
- ²⁹C. Raufaste, A. Foulon, and B. Dollet, Dissipation in quasi-two-dimensional flowing foams, *Phys. Fluids* **21**, 053102 – 053110 (2009).
- ³⁰B. Dollet, Local description of the two-dimensional flow of foam through a contraction, *J. Rheol.* **54**, 741 (2010).
- ³¹B. Dollet and F. Graner, Two-dimensional flow of foam around a circular obstacle: local measurements of elasticity, plasticity and flow, *J. Fluid Mech.* **585**, 181–211 (2007).
- ³²W. Drenckhan, S. Cox, G. Delaney, H. Holste, D. Weaire, and N. Kern, Rheology of ordered foams—on the way to Discrete Microfluidics, *Colloids Surf. A* **263**(1-3), 52 – 64 (2005).

- ³³V. R. Guillen, M. I. Romero, M. da Silveira Carvalho, and V. Alvarado, Capillary-driven mobility control in macro emulsion flow in porous media, *Int. J. Multiphas. Flow* **43**, 62–65 (2012).
- ³⁴J.-P. Raven and P. Marmottant, Periodic microfluidic bubbling oscillator : insight into the stability of two-phase microflows, *Phys. Rev. Lett.* **97**, 154501 (2006).
- ³⁵T. Green, P. Grassia, L. Lue, and B. Embley, Viscous froth model for a bubble staircase structure under rapid applied shear: An analysis of fast flowing foam, *Colloids Surf. A* **348**, 49 – 58 (2009).
- ³⁶K. Brakke, The Surface Evolver., *Exp. Math.* **1**, 141–165 (1992).
- ³⁷H. Bruus, *Theoretical Microfluidics*, Oxford University Press, Oxford, 2008.
- ³⁸B. Dollet and I. Cantat, Deformation of soap films pushed through tubes at high velocity, *J. Fluid Mech.* **652**, 529–539 (2010).